JOURNAL OF PROPULSION AND POWER
Vol. 13, No. 5, September–October 1997

Performance Optimization of a Supersonic Combustion Ram Accelerator Projectile

John W. Sabean* and Mark J. Lewis†
University of Maryland, College Park, Maryland 20742-3015

The optimization of a supersonic combustion ram projectile shape, using a computational analysis, is presented. A projectile flying at hypersonic speed is passed through a combustible mixture. Shocks generated by a ring cowl surrounding the projectile ignite the flow over the projectile tail, causing it to accelerate. This method could be used to accelerate projectiles to velocities in excess of 2.7 km/s. The thrust and drag forces on such a projectile are very large and are of the same order of magnitude. Small changes in the projectile design can have a large effect on the net thrust acting on the projectile. A computational analysis using an inviscid computational fluid dynamics (CFD) code, including chemical reactions, is linked to a gradient-based optimizer. The projectile is then optimized for maximum thrust at several different Mach numbers. Multiple CFD solutions are used to generate a thrust curve used in optimization for other design functions, such as maximum velocity and minimum accelerator tube length. All configurations are compared to determine the best configuration for practical use. Optimized configurations are capable of higher velocities, but the main benefit gained is the reduction in the length required to reach that maximum velocity.

Nomenclature

A = cross-sectional area of ring cowl
a = length of projectile nose
b = projectile centerbody throat length
C_t = thrust coefficient, F/PA
E_a = activation energy
F = net force on projectile
g = ring cowl length
K = chemical reaction rate constant
k = ring tail angle
l-o = Bezier control point coordinates for tail shape
P = pressure
Q = nondimensional chemical heat release, q/C_pT
R = specific gas constant
s = ring cowl position
T = temperature
$[X]$ = molar concentration of species X, kg-mole/m^3

Introduction

THE supersonic combustion ram (SCRAM) accelerator is a method for accelerating projectiles through a premixed fuel/oxidizer mixture, by using the shock waves generated by the projectile to detonate the mixture. The SCRAM accelerator consists of a launch gun, which injects the projectile into the fuel/oxidizer mixture at a velocity of 2.3 km/s. The shock waves generated by a ring cowl surrounding the projectile initiate combustion in the mixture, while the remaining mixture combusts over the rear portion of the projectile. The high-pressure flow over the tail of the projectile results in a net positive thrust, accelerating the projectile to higher velocities through the mixture. This configuration, along with the external propulsion accelerator concept, were initially proposed by Rom et al.[1] The focus of this work is on the shape optimization of the SCRAM configuration (Fig. 1).

The SCRAM accelerator is similar to the ram accelerator, developed at the University of Washington.[2] A projectile is injected into an accelerator tube that contains a high-pressure premixed fuel/oxidizer mixture and acts as a centerbody of a ramjet; whereas the accelerator barrel acts as a long cowling. The interaction of the cone shock with the barrel walls and the projectile initiate the combustion, accelerating the projectile through the barrel. As with a ramjet, the projectile is limited to lower Mach numbers, and higher velocities can only be reached by raising the speed of sound of the mixture. The ring configuration, however, is more analogous to a supersonic combustion ramjet, or scramjet. All of the combustion takes place in a supersonic region, allowing for positive thrust at higher Mach numbers to be achieved. However, there is a tradeoff in that the combustion process tends to be less efficient, and the characteristic thrust levels are lower than that of a ram accelerator. The thrust levels may be lower; however, positive thrust can still be achieved at higher Mach numbers, suggesting that higher maximum velocities may be possible if there are no restrictions on the accelerator tube length. A SCRAM accelerator would also allow for supersonic combustion testing, making it a potentially good tool for scramjet research.

Initial calculations show that the magnitude of both the thrust generated and the drag are both on the order of 30 kN. Both values are large and the difference results in a net thrust on the order of 2–3 kN. As a result, small changes in the geometry of the projectile can produce large changes in the amount of net thrust produced. Hence, this problem is a good candidate for shape optimization.

The computational requirements to calculate the thrust on one of these projectiles are considerable. The only way to accurately model the flowfield over the projectile, with respect to its shape, is by utilizing a computational fluid dynamics (CFD) code that includes finite rate chemical reactions. Because of the large number of grid points needed and the number of chemical reactions necessary for a full methane–air model, the CPU time necessary for one calculation, even using a supercomputer, can be 3–5 CPU hours.[3,4] An optimizer typically requires 50–100 individual CFD calculations to converge the optimizer on a design, making such chemistry mod-

Presented as Paper 96-2950 at the AIAA/ASME/SAE/ASEE 32nd Joint Propulsion Conference, Lake Buena Vista, FL, July 1–3, 1996; received Oct. 1, 1996; revision received April 1, 1997; accepted for publication April 2, 1997. Copyright © 1997 by the American Institute of Aeronautics and Astronautics, Inc. All rights reserved.

*Graduate Research Assistant, Department of Aerospace Engineering. Student Member AIAA.

†Associate Professor, Department of Aerospace Engineering. Associate Fellow AIAA.

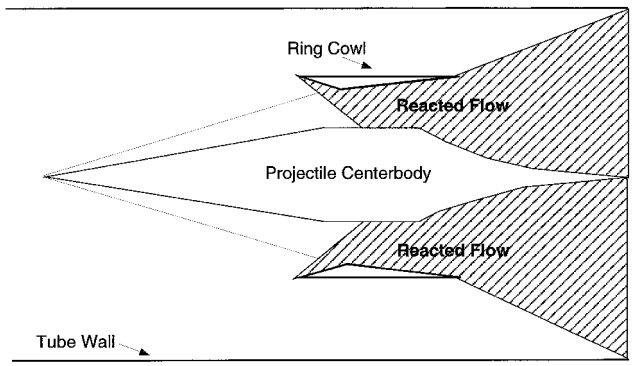

Fig. 1 SCRAM configuration.

els undesirable for this application. However, as shown in this work, by simplifying the chemistry model, an accurate calculation can be achieved in a reasonable amount of time for use with an optimizer.

Numerical Formulation

Computational Scheme

The computations in this work are performed using the General Aerodynamic Simulation Program (GASP).[5] This code is used to solve the axisymmetric Euler equations, including finite rate chemical reactions. This solution is intended for use in an optimizer, and an inviscid flow was assumed for faster convergence. The pressures used in the SCRAM accelerator are on the order of 50 atm, and as such, the pressure forces far exceed the viscous forces. It should be noted, however, that viscous effects may very well be significant. The Reynolds numbers for this flow are on the order of 3×10^9, and as such, the flow is most likely turbulent. Shock/boundary-layer interactions may occur, inducing flow separation inside the ring. The significance of these viscous effects should be addressed in future work, but have been neglected for purposes of this investigation.

The flowfield is supersonic at all points in the calculation, and space marching can be used to decrease the amount of time required to obtain a solution. The full flux can be used in the marching direction i, with catastrophic limiting of the mixture density and pressure, in which a first-order interpolation is used if either of these values becomes negative for a particular cell face. The spacial accuracy was a second-order-accurate extrapolation in the upwind direction. In the radial direction j, GASP is set to use Roe's flux-difference splitting and a superbee limiter.[5] The time integration is done implicitly using a first-order-accurate LU decomposition on a single line, for a constant value of i, with relaxation in the sweep direction. Using space marching greatly reduces the cost of obtaining a solution. The solution was run until the residual decreased six orders of magnitude before passing the result to the optimizer.

All calculations were done with fixed initial conditions that represent proposed testing conditions at the Army Research Labs ram accelerator facility in Aberdeen, Maryland. The projectile was designed with a 60-mm ring diameter, approximately 250 mm long, and would fly in a 120-mm-diam tube. The mixture was chosen as the one with the highest heat release Q, which would not result in an unstart at Mach 6.4, the injection Mach number, based on numerical calculations with various test geometries. The initial conditions are 1) $P_{\text{inf}} = 50$ atm, 2) $T_{\text{inf}} = 300$ K, and 3) mixture: $2.1CH_4 + 2O_2 + 10.0N_2$.

Chemistry Model

The choice of a chemistry model is limited by the resulting computational cost of the CFD solution. Use of a methane–air model, such as proposed by Yungster and Rabinowitz,[6] is more accurate; however, it consists of 19 reacting species and 52 elementary reactions. Implementation of this mechanism, however, would require tens of CPU hours per computational solution, making it undesirable for use in an optimization problem. Therefore, the less computationally intense model of Westbrook and Dryer,[7] a global chemistry model, is used in the present effort.

One of these global models has been explored by Nusca,[8] to determine its accuracy for use in ram accelerator calculations, in comparison to more detailed models and experimental data. The ignition times found in experiments done by Petersen et al.[9] cannot be directly compared with the global model, because of its almost instantaneous ignition time. Looking at this data, using the pressure and temperature data for a nonreaction flow over a SCRAM projectile with the same chemical properties, the ignition time is on the order of 10^{-6}–10^{-7} s. With a flow velocity on the order of 2 km/s, the distance the ignition occurs over would be on the order of 1–2 mm. A global kinetics mechanism with an instantaneous ignition time should give a sufficient approximation of the performance.

The model chosen for the present work was the two-step chemistry model instead of the one-step model. This selection provides lower computational costs and takes into account more of the intermediate species that will be present in the flow. This mechanism is given as[7]

$$CH_4 + \tfrac{3}{2}O_2 \Rightarrow CO + 2H_2O \tag{1}$$

$$CO + \tfrac{1}{2}O_2 \Leftrightarrow CO_2 \tag{2}$$

The rate expression for the first step is a modified Arrhenius formulation, where the constants a and b where chosen to fit results from flame experiments using larger kinetic mechanisms[7] (all constants are in kilograms, moles, meters, seconds, and Kelvin):

$$K_{\text{OV}} = AT^n \exp[(-E_a)/RT](\text{Fuel})^a(\text{Oxidizer})^b \tag{3}$$

with the following constants:

$$A = 1.5 \times 10^7, \qquad n = 0.0$$
$$E_a = 15{,}119, \qquad a = -0.3, \qquad b = 1.3 \tag{4}$$

The second reaction [Eq. (2)], requires a different formulation for both a forward and a backward rate. These are given as

$$K_{CO_2\,\text{forward}} = 1.26 \times 10^{10} \exp[(-20143)/RT](CO)^1(H_2O)^{0.5}(O_2)^{0.25} \tag{5}$$

$$K_{CO_2\,\text{backward}} = 5.00 \times 10^8 \exp[(-20143)/RT](CO_2)^1 \tag{6}$$

Reaction mechanisms with more equations were also considered for this work; however, these were more computationally intensive. An equilibrium analysis including all species suggests that this simplification results in a slight overprediction in the value of C_t, though the trends in the optimization should remain the same. As such, the two-step reaction mechanism was the best choice for use with the optimizer.

Grid Determination

The grid dimensions chosen for these computations are shown in Table 1. The various computational zones are shown in Fig. 2. No grid was generated above the grid cowl, because the cowl was oriented parallel to the flow and would have no effect as a result of the inviscid flow assumption. The flow in this section is set to freestream properties and allowed to interact with the flow exiting the ring in zone 3.

These grid dimensions were chosen based on a grid-dependence study, and analyzed for the sensitivity of the value of C_t to grid size. The dimensions of the grid in Table 1 were doubled, and the computed value of C_t for the fine grid was

Table 1 Grid dimensions for each computational zone

Zone	*I* dimension	*J* dimension
1	75	70
2	100	70
3	70	110

compared to the value for the original grid. Although the error in the individual contributions to the value of C_t for each zone is relatively small, the error in the computed net thrust is quite large, because of truncation error. The maximum difference in the individual contributions for each zone, between the fine grid and the normal, was 5.6%, demonstrating that the pressure distribution over each surface was fairly accurate. The largest total difference in the value of C_t, between a fine grid and a normal grid, was 35%. This posed a challenge because the optimizer requires a very accurate value of C_t to properly calculate the search direction. It was determined, however, that this large error was mainly a result of the value of the drag on the ring. However, the pressure on this portion of the projectile was the only part that appeared to be sensitive to the grid size. This value remains constant throughout the optimization because the shape of the ring forebody is fixed and never intersects with the nose shock. When the optimizer calculates the gradients, this constant value is subtracted out. When taking this factor into account, the total difference in the value of (C_t–ring forebody drag) is reduced to less than 1%. This proved sufficient for use with the optimizer, except when the value of C_t is close to zero. As the value of C_t approaches zero, both the wave drag and the thrust acting on the projectile are almost equal, and they are very large in value. The truncation error involved in subtracting these two numbers becomes very significant as the difference of the two values approaches zero.

Optimization Formulation

Optimization Method

The optimization was performed utilizing the design optimization tools (DOT) software package, by VMA Engineering.[10] The software was set to use the Broydon–Fletcher–Goldfarb–Shanno (BFGS) search direction algorithm, which is a quasi-Newton method that finds the search direction by approximating the inverse of the Hessian matrix. The BFGS algorithm is chosen because of its theoretically faster convergence. The gradients used in the algorithm were calculated using finite differences. For this study, the number of design variables was limited to 9, and the cost of calculating the finite differenced gradients was not severe. However, in a study with more design variables, the use of a sensitivity analysis, as proposed by Burgreen et al.,[11] would be a more efficient way of computing the gradients, and a BFGS algorithm could still be used.

Design Variable Formulation

The shape of the ring front was chosen to be a power law body that would generate combustion at the entrance Mach number with minimum drag. The entrance Mach number was chosen to be 6.4. A projectile designed for a lower entrance Mach number would not maintain positive thrust over a very long range of Mach numbers. Higher entrance Mach numbers would be desirable, but they challenge the capabilities of launcher technology. The ring thickness was minimized, to minimize the drag caused by the ring forebody. This ring thickness value was fixed so that the ring could contain the high pressure associated with combustion. The ring cowl radius was fixed as well, to maintain the overall size of the projectile.

The nine design variables chosen for this work are shown in Fig. 2. Five of the design variables are the physical dimensions of the projectile. The nose was determined by a third-order polynomial. The radius of the nose was fixed to 15 mm, while the a was allowed to vary. The remainder of these five variables were used to determine the relative positions and lengths of the ring and the base projectile.

The other four variables are used with a fourth-degree Bezier–Bernstein curve to determine the shape of the tail, based on an idea proposed by Burgreen et al.[11] The two end control points are fixed, and two control points in the middle are allowed to move in both the X and Y directions, as given by design variables: *l*-*o*. By utilizing such a curve, a wide variety of shapes can be produced using only a few Bezier control points. The locations of the points on a nth-deg Bezier–Bernstein curve are given by

$$X_b(u) = \sum_{k=0}^{n} B_{k,n}(u) P_k \qquad 0 \le u \le 1 \tag{7}$$

where

$$B_{k,n}(u) = \frac{n!}{k!(n-k)!} u^k (1-u)^{n-k} \tag{8}$$

P_k represents the coordinates of the Bezier control points, and X_b is the point located at the nondimensional distance u, along the curve.

The flow in the region of a blunt case, as used in traditional ram accelerator projectiles, would be near stagnation,[12] and the high total temperatures associated with the higher Mach numbers in a SCRAM accelerator would produce a large amount of dissociation, resulting in the loss of combustion energy. A contoured shape, however, would provide for an isentropic compression of the flow on the tail, increasing the thrust and conserving the combustion energy. Therefore, a contoured shape was chosen for the tail, as opposed to a blunt base.

Optimization Architecture

Normally, to couple a computational code with an optimizer, both programs are run on the same machine, with the optimizer calling the computational code as needed for evaluating the chosen objective function. Although this can be easily implemented for an optimization where only a single CFD solution is required for one objective function evaluation, it is not the most efficient choice for an objective function evaluation that requires multiple CFD solutions. A better answer is to divide the task up and calculate the multiple CFD solutions on separate processors or machines. The optimization code, which is not very computational intensive, can be run on a lower-powered machine. For the present study, a SPARC 5 workstation was used. When a function evaluation is required, a single computational grid is obtained. The controlling program spawns GASP processes on several DEC Alpha workstations. The controlling process monitors the progress of the CFD solutions, collects the results from the other machines, and computes the objective function based on these results. A flow chart for this multiple CFD solution configuration can be found in Fig. 3.

This architecture allows the CFD processes to run in parallel, providing a faster overall run time. A typical solution would require 1.5–2 CPU hours on an Alpha 3000/300 workstation, or about 40 CPU min on an AlphaStation 600/266. With an optimizer requiring up to 100 of these calculations, using a single computer to calculate multiple solutions would increase the run time required by several days, possibly several weeks. For this study, the optimizer made use of three CFD solutions to generate an acceleration curve, which is then used to calculate either the minimum tube length required to achieve a certain velocity or the maximum velocity a projectile can reach. Given more resources, more CFD solutions could be

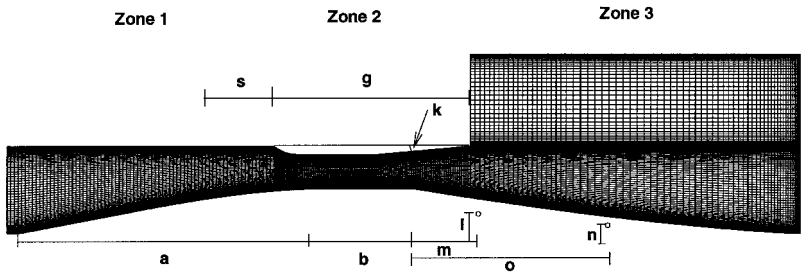

Fig. 2 Design variables for optimization.

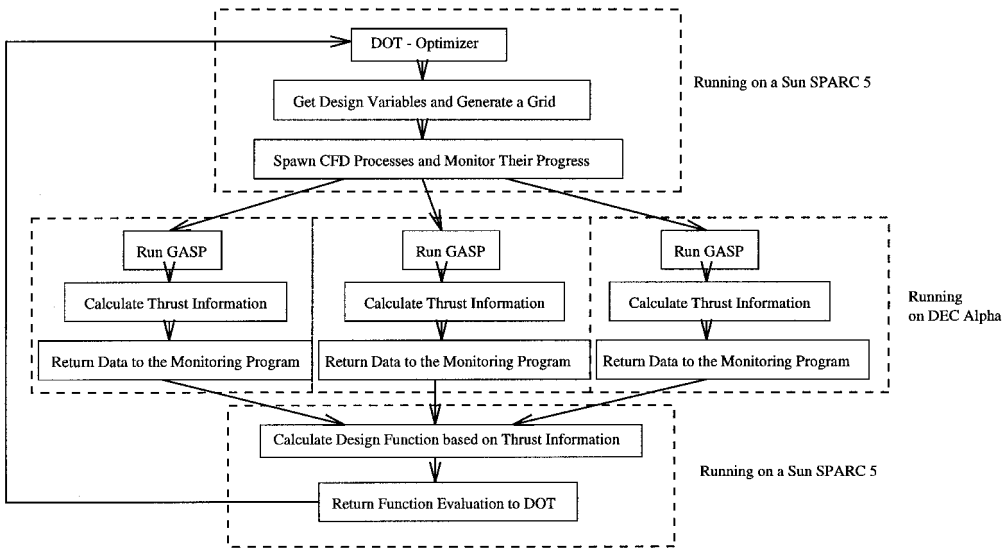

Fig. 3 Flow chart for multiple Mach number optimization.

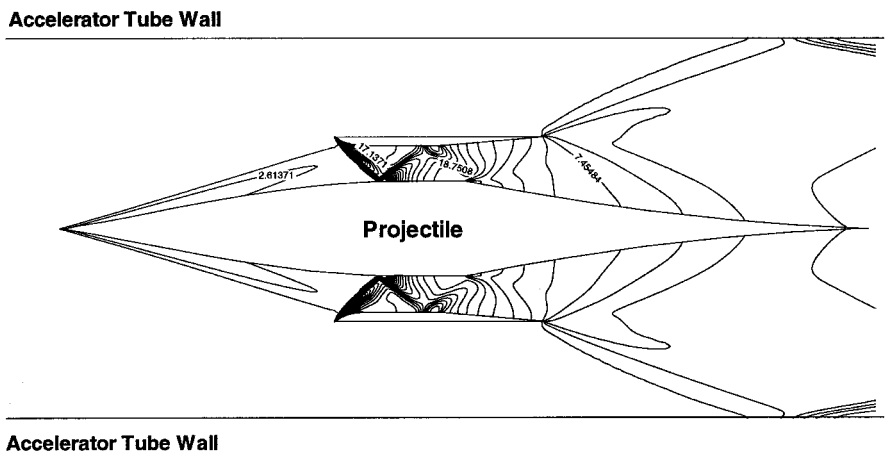

Fig. 4 Pressure contours at Mach 6.4 for Mach 6.4 optimized configuration.

calculated to increase the accuracy of the acceleration curve while maintaining the same overall run time.

Results

Various optimization runs were performed using different objective functions and design conditions. The primary focus was optimizing for maximum thrust at a single Mach number, and optimizing projectile performance over several Mach numbers. These two objectives are analyzed separately and compared to determine which objective functions and methods will produce a desired benefit.

Single Mach Number Optimizations

For the single Mach number optimizations, the projectile was optimized for maximum C_t. Optimization runs were done for three Mach numbers that spanned the approximate operational range of a projectile with the chosen ring shape. The projectile was designed such that the flow would ignite starting at Mach 6.4 and continue to have positive thrust until approximately Mach 7.6. Single Mach number optimizations were performed at Mach 6.4, 7.0, and 8.0.

The pressure contours for the final optimized configurations are shown in Figs. 4–6. The most important parameters in these optimizations are s, g, and b. These parameters control where the shock reflections occur inside the ring. The optimized configurations are where the reflected shock waves cancel the expansion waves that occur inside the ring. For the Mach 6.4 case, the reflected shock cancels the expansion waves that occur at the beginning of the projectile tail (Fig. 4). However, in the Mach 7.0 and 8.0 cases, the optimized

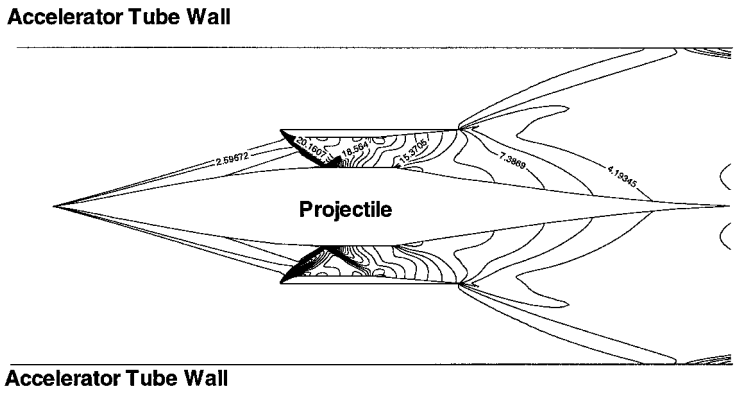

Fig. 5 Pressure contours at Mach 7.0 for Mach 7.0 optimized configuration.

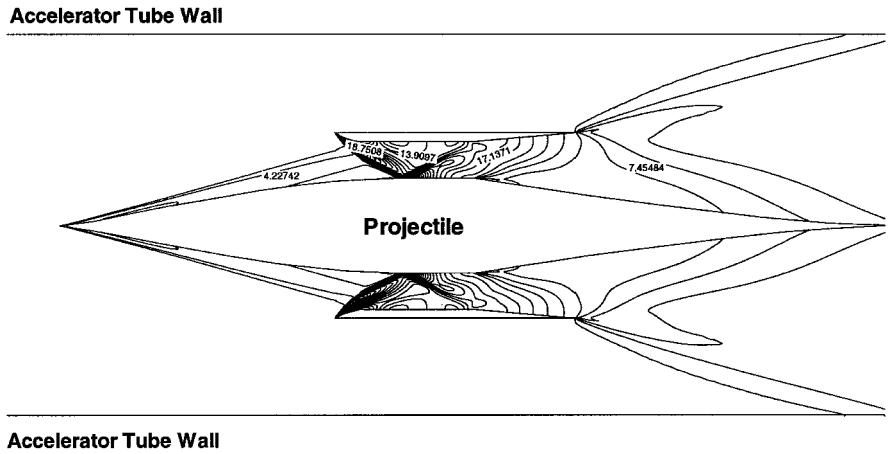

Fig. 6 Pressure contours at Mach 8.0 for Mach 8.0 optimized configuration.

configuration is one where it is more beneficial to cancel the expansion waves that occur at the beginning of the ring tail (Figs. 5 and 6). At the lower Mach numbers, the performance lost as a result of the expansion at the ring tail is less significant than performance gained by canceling the expansion at the beginning of the projectile tail. At the higher Mach numbers, the expansion at the ring tail is stronger and its effects become more significant. As the optimization progresses, the ring tail expansion region is improved while performance at the projectile tail expansion is sacrificed.

It is important to note that the projectile tail is fairly straight in all of the optimized configurations. The Bezier curve provides substantial variability over this shape; however, the shape remains relatively flat in the optimized configurations. This is mainly because a large expansion at the beginning of the tail would be necessary to make use of the isentropic compression, but this would reduce the pressure. Because the projectile is axisymmetric, the loss of pressure at the top of the tail has a relatively large effect on the total thrust because there is more surface area in this region. A higher pressure can be generated toward the end of the tail with a contoured shape; however, the surface area is reduced so that it has little effect on the overall thrust. The optimized configuration tends to be a long tail with a shallow expansion at the beginning of the tail.

Multiple Mach Number Optimizations

The multiple Mach number optimizations were performed for two objective functions: 1) maximum velocity and 2) minimum tube length. The maximum velocity optimization was done using the thrust curve to determine the maximum velocity the projectile was capable of achieving. The minimum tube length optimization was accomplished by using the thrust curve with a kinematic calculation to determine the length of tube necessary to accelerate the projectile to 2.7 km/s. Both of these optimizations used three CFD solutions, using the same projectile geometry to approximate a thrust curve, which was curve fit with a second-order polynomial. A sample curve is shown in Fig. 7. The curve is a good approximation for the lower Mach numbers, but as the thrust coefficient approaches zero, the accuracy of the thrust curve diminishes because of the large truncation error. This curve was accurate enough to produce a converged solution for the maximum velocity optimization; however, it was not accurate enough to obtain an absolute optimum for the minimum tube length calculation.

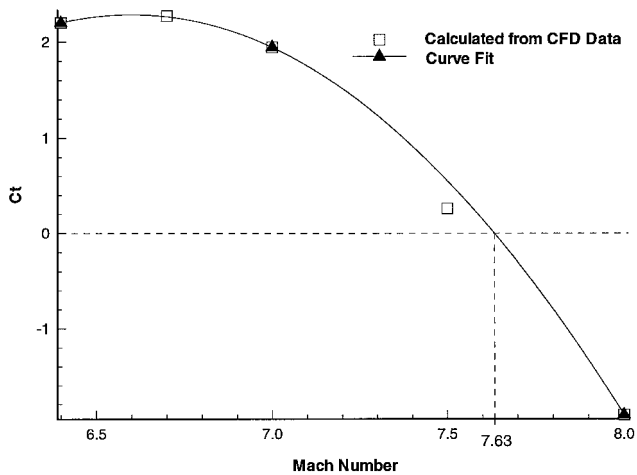

Fig. 7 Sample thrust vs Mach number curve for multiple Mach number optimizations.

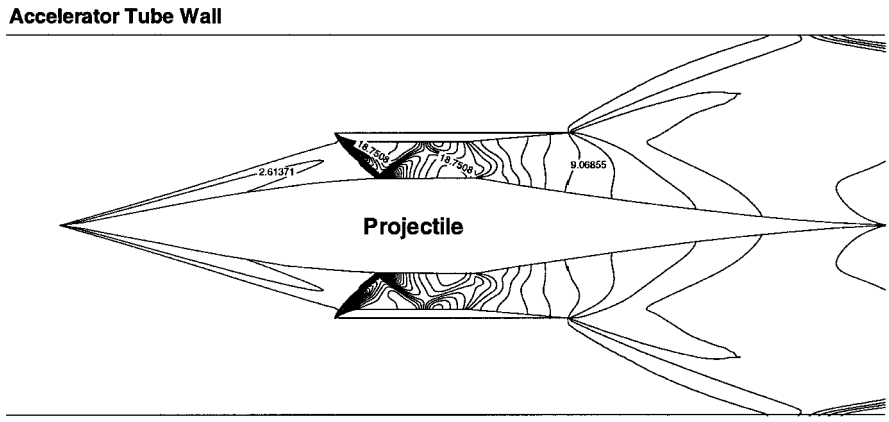

Fig. 8 Pressure contours at Mach 6.4 for maximum velocity optimized configuration.

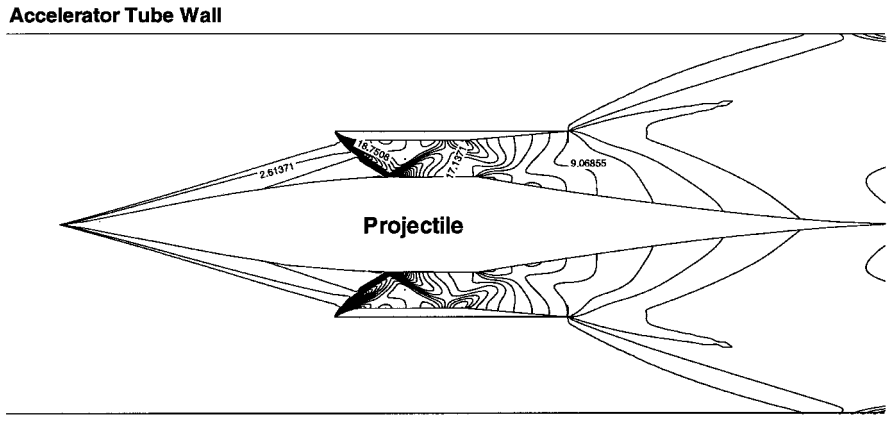

Fig. 9 Pressure contours at Mach 7.0 for maximum velocity optimized configuration.

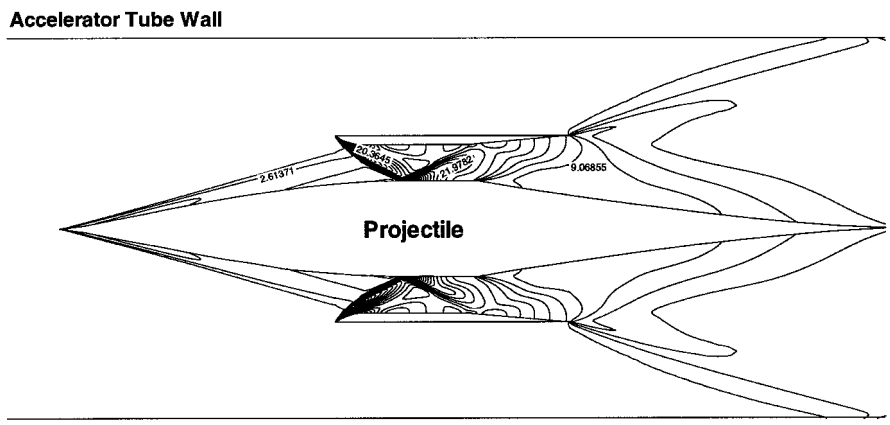

Fig. 10 Pressure contours at Mach 8.0 for maximum velocity optimized configuration.

The minimum tube length optimization results presented here represent a local minimum, but one that reduced the tube length significantly from an initial value.

The actual computations of the maximum velocity and tube length were done using the thrust curves and the computed volume of the given projectile design. The mass of the projectile was determined by making the conservative assumption of a solid projectile made of stainless steel. This produced projectile masses on the order of 0.8 kg. Construction of an actual projectile would involve making parts of the projectile hollow, and possibly the use of other materials with lower densities. The projectile acceleration would improve by an amount proportional to the mass reduction, and as such, the results presented here could be scaled appropriately.

The pressure contours for the final, optimized configurations are shown in Figs. 8–13. In the maximum velocity-optimized configuration, the Mach number where the value of C_t becomes zero is increased to raise the overall velocity of the projectile. As the optimization progresses, the values of C_t at Mach 7.0 and 8.0 are raised, while the performance at Mach 6.4 is decreased. As can been seen in Figs. 8–10, the optimizer behaves in a manner similar to that of the single Mach number optimizations. The optimum value of C_t for both Mach 7.0 and 8.0 occurs when the reflected shock cancels the expansion

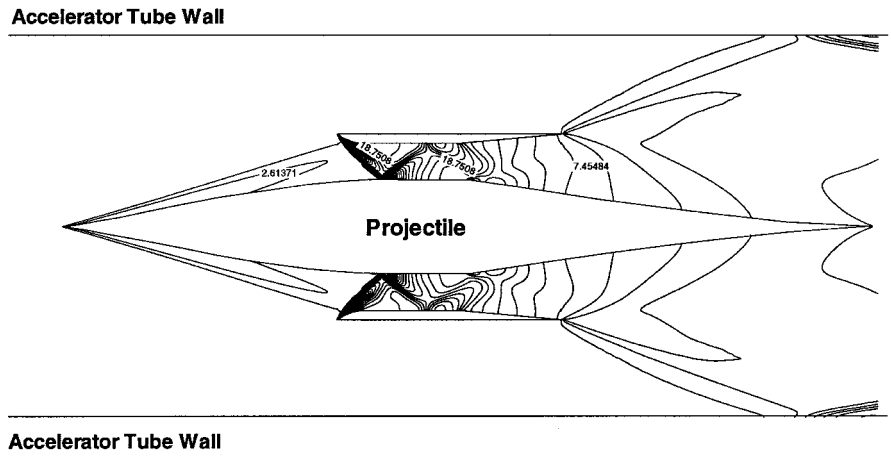

Fig. 11 Pressure contours at Mach 6.4 for minimum tube length optimized configuration.

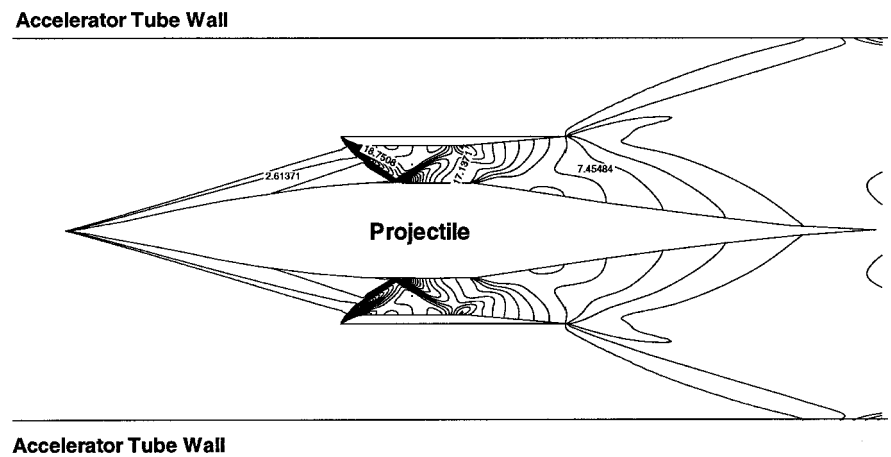

Fig. 12 Pressure contours at Mach 7.0 for minimum tube length optimized configuration.

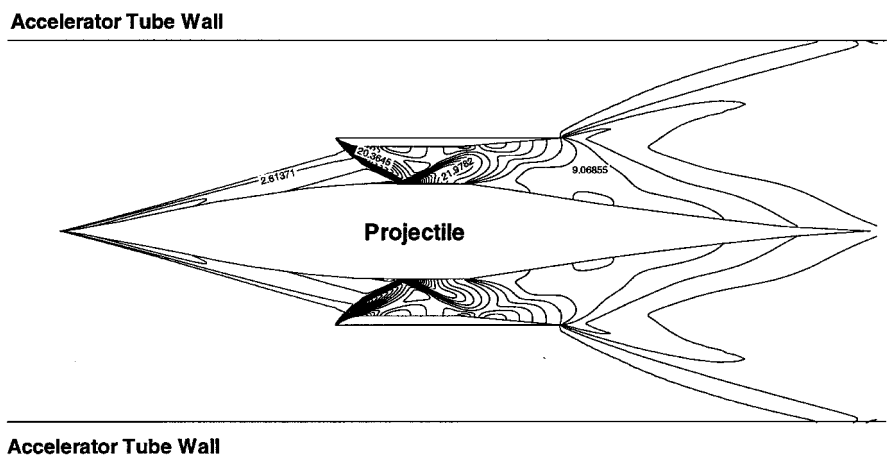

Fig. 13 Pressure contours at Mach 8.0 for minimum tube length optimized configuration.

waves that occur at the beginning of the ring tail. The optimized configuration is one that lies between these two Mach numbers. The shock lands just before this corner (Fig. 9), and lands just after the corner in Fig. 10. In both cases, the shock partially cancels the expansion waves, but the optimal configuration lies between the two Mach numbers near the maximum Mach number of 7.68.

The minimum tube length optimization did not converge to a global minimum; however, the tube length was reduced significantly. The initial configuration to this optimization was the optimized maximum velocity configuration, and so the results are similar. The initial tube length required to reach a velocity of 2.7 km/s was approximately 200 m. This tube length was reduced by the optimizer to approximately 150 m. This is accomplished by factoring in the value of C_t at Mach 6.4, which the maximum velocity optimization had sacrificed. As can be seen in Fig. 11, this configuration is closer to the single Mach number optimization configuration, where the reflected shock lands on the expansion corner at the beginning of the projectile tail. Because this design is close to the maximum velocity

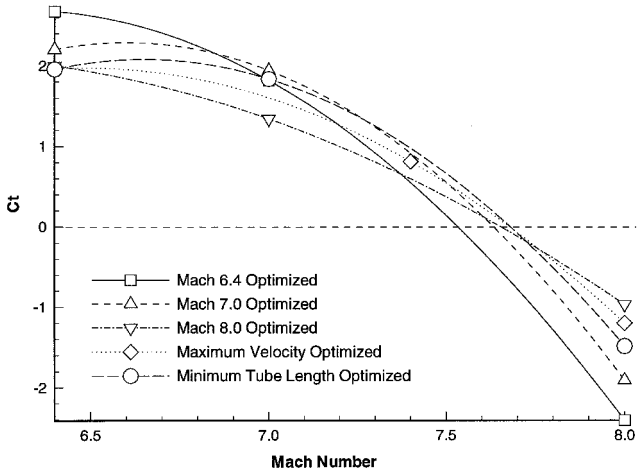

Fig. 14 Thrust vs Mach number for optimized configurations.

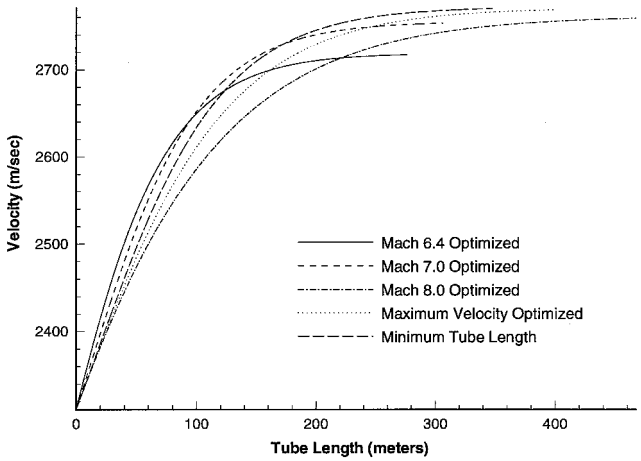

Fig. 15 Distance vs velocity for optimized configurations.

design, the balance between the value of C_t at both Mach 7.0 and 8.0 still exists (Figs. 12 and 13). This may not be the global optimum, but it does present a good balance between tube length and maximum velocity.

Results for the performance of all the optimized configurations are shown in Figs. 14 and 15. Figure 14 shows that the overall maximum Mach number for each optimization seems to be approaching an upper limit with both single and multiple Mach number methods. This suggests that optimization applied to increase the maximum velocity will only have limited benefits for a given basic design. The drag on the ring is the major obstacle toward reaching a higher maximum Mach number.

Conclusions

This work used a computational analysis in conjunction with an optimizer to improve the performance of SCRAM accelerator projectile designs. The choice of an objective function had a significant effect on the benefits of optimization. Although improvements in the overall maximum velocity of these projects could be made, it was found that these improvements were small compared to the average velocity of the projectile. The design parameters chosen had only a small effect on the maximum velocity. The main parameter in determining maximum velocity appears to be the drag on the ring forebody. A better option to increasing the maximum velocity would be to increase the value of Q by changing the mixture. This higher value of Q could not be used at the injection Mach number of 6.4; however, it could be used in a second stage after the projectile has accelerated to a higher velocity.

Better performance is achieved by optimizing the design for minimum accelerator tube length. In both the single Mach number optimizations and the minimum tube length optimization, it was shown that the accelerator tube length required to accelerate a projectile to its maximum velocity varied up to 50%; whereas the corresponding maximum velocity varied only 5–10%. With only a small sacrifice in maximum velocity, the accelerator tube length can be shortened a great deal.

The choice of using a multiple Mach number optimization against using a single Mach number optimization also has an effect on the performance of the final design. As expected, for the single Mach number optimizations, the shape of the thrust curve changed significantly, depending on the chosen Mach number. For low Mach numbers, the projectile had a high initial thrust, but a lower maximum velocity. For the high Mach numbers, the projectile could sustain positive thrust at a higher velocity; however, the thrust was lower at the low Mach numbers, and accelerating to that velocity took much longer. A good balance was achieved by optimizing for thrust at a Mach number near the middle of the operational range of the projectile. Using a multiple Mach number optimization, although more time consuming and resource intensive, solves the problem of guessing where optimal performance would occur. This was shown in the maximum velocity optimization, where the optimum design point appeared to be between Mach 7.0–8.0. Although the minimum tube length optimization did not converge to a global minimum, it also showed the benefits of taking into account the entire thrust curve in determining optimal performance. The choice between multiple Mach number optimization and single Mach number optimization is a tradeoff between performance and computational resources. A single Mach number optimization can produce good results; however, the added resources of a multiple Mach number optimization can improve the overall performance of the projectile.

Acknowledgments

This work was supported, in part, by the Center of Hypersonic Education and Research, NASA NAGw 11796; Isaiah Blankson was the Technical Monitor, to whom appreciation is expressed. The authors thank Josef Rom for all of the help and advice he provided. Thanks also go to Ashwani K. Gupta at the Department of Mechanical Engineering, at the University of Maryland, for his technical expertise and support. Gratitude is also expressed to James Randolph at the Supercomputing Center at the Jet Propulsion Laboratory for the generous allocation of CRAY time. Appreciation is also expressed to Josh Elvander and Carl Knowlen, at the University of Washington, for providing the code used to calculate various mixture properties. Thanks also go to Michael Nusca and David Kruczynski for providing information about the testing conditions at the HIRAM facility at Army Research Laboratory in Aberdeen, Maryland.

References

[1]Rom, J., Lewis, M., Gupta, A., and Sabean, J., "Hypersonic Aerodynamics Test Facility Using the External Propulsion Accelerator," AIAA Paper 95-6138, April 1995.

[2]Hertzberg, A., Bruckner, A., and Bogdanoff, D., "Ram Accelerator: A New Chemical Method for Accelerating Projectiles to Ultrahigh Velocities," *AIAA Journal*, Vol. 26, No. 2, 1988, pp. 195–203.

[3]Nusca, M., "Reacting Flow Simulations for a Large Scale Ram Accelerator," AIAA Paper 94-2963, June 1994.

[4]Grismer, M., and Powers, J., "Calculations for Steady Propagation of a Generic Ram Accelerator Configuration," *Journal of Propulsion and Power*, Vol. 11, No. 1, 1995, pp. 105–111.

[5]McGrory, W. D., Slack, D. C., Applebaum, M. P., and Walters, R. W., *GASP Version 2.2*, Aerosoft, Inc., Blacksburg, VA, 1993.

[6]Yungster, S., and Rabinowitz, M., "Numerical Study of Shock-Induced Combustion in Methane-Air Mixtures," AIAA Paper 93-1917, June 1993.

[7]Westbrook, C., and Dryer, F., "Chemical Kinetic Modeling of Hydrocarbon Combustion," *Progress in Energy Combustion Science*, Vol. 10, 1984, pp. 1–57.

[8]Nusca, M., "Investigation of Ram Accelerator Flows for High Pressure Mixtures of Various Chemical Compositions," AIAA Paper 96-2946, July 1996.

[9]Petersen, E., Davidson, D., and Hanson, R., "Ignition Delay Times in Ram Accelerator Mixtures," AIAA Paper 96-2681, July 1996.

[10]Engineering, V., *DOT User Manual, Version 4.00*, Vanderplaats, Miura and Associates, Inc., Goleta, CA, 1993.

[11]Burgreen, G., Baysal, O., and Eleshaky, M., "Improving the Efficiency of Aerodynamic Shape Optimization," *AIAA Journal*, Vol. 32, No. 1, 1994, pp. 69–76.

[12]Grasso, F., and Pettinelli, C., "Analysis of Laminar Near-Wake Hypersonic Flows," *Journal of Spacecraft and Rockets*, Vol. 32, No. 6, 1995, pp. 970–980.